Vanadium distribution between forsterite and its melt: The structural and oxidation state of vanadium

Article *in* Geochemistry International · July 2001

CITATIONS
6

READS
61

6 authors, including:

V. B. Dudnikova
Lomonosov Moscow State University
48 PUBLICATIONS **179** CITATIONS
SEE PROFILE

Evgeny Vasilievich Zharikov
Russian Academy of Sciences
376 PUBLICATIONS **2,378** CITATIONS
SEE PROFILE

N. N. Eremin
Lomonosov Moscow State University
108 PUBLICATIONS **427** CITATIONS
SEE PROFILE

Vyacheslav Fedorovich Lebedev
ITMO University
120 PUBLICATIONS **262** CITATIONS
SEE PROFILE

Geochemistry International, Vol. 39, No. 7, 2001, pp. 667–675. Translated from Geokhimiya, No. 7, 2001, pp. 734–743.

Vanadium Distribution between Forsterite and Its Melt: The Structural and Oxidation State of Vanadium

V. B. Dudnikova[1], E. V. Zharikov[2, 3], N. N. Eremin[1, 4], E.V. Zharkova[1], V. F. Lebedev[2], and V. S. Urusov[1, 4]

[1] *Vernadsky Institute of Geochemistry and Analytical Chemistry, Russian Academy of Sciences, ul. Kosygina 19, Moscow, 117975 Russia*

[2] *General Physics Institute, Russian Academy of Sciences, ul. Vavilova 38, Moscow, 117942 Russia*

[3] *Mendeleev University of Chemical Technology, Miusskaya pl. 9, Moscow, 125047 Russia*

[4] *Geological Division, Moscow State University, Vorob'evy gory, Moscow, 119899 Russia*

Received June 8, 2000

Abstract—Forsterite single crystals doped with vanadium were grown from melt using the Czochralski technique in various oxidation–reduction conditions: nitrogen, nitrogen with oxygen, argon, and argon with hydrogen atmospheres. The forsterite crystal/melt distribution coefficient is 0.07. Spectra of optical absorption within the range of 350–1600 nm, luminescence spectra, and the dependence of crystal density on vanadium content were studied. A thermodynamic analysis of the most probable oxidation state of vanadium together with a computer simulation of the forsterite crystal structure were also performed. A comprehensive study revealed that the forsterite crystals synthesized by the Czochralski technique mainly contain tetravalent vanadium, which substitutes for silicon. The oxidation state of this element can be changed to V^{3+} or V^{5+} by annealing the crystals under reducing or oxidizing conditions, respectively.

INTRODUCTION

Vanadium occurs in various oxidation states, and its ions can occupy the following sites in the forsterite crystal structure: two types of Mg-octahedra, M1 (C_i symmetry) and M2 (C_s symmetry), and Si-tetrahedra (C_s symmetry). The M1 octahedron is smaller than the M2 octahedron. The ionic radii (r) of V^{2+} and V^{3+} in eightfold coordination are 0.79 and 0.64 Å, while $r(Mg^{2+})$ is 0.72 Å [1]. In fourfold coordination, the ionic radius of V^{5+} is 0.36 Å, while that of Si^{4+} is 0.26 Å. The ionic radius of V^{4+} in fourfold coordination can be estimated by extrapolation of the $r(V^{4+})$ dependence on the coordination number and is 0.46 Å.

The vanadium content in natural olivine is low, up to 35 ppm [2]. The vanadium distribution coefficients between the olivine and silicate melt vary with temperature, pressure, melt composition, and oxygen fugacity (f_{O_2}) and range from 0.04 [3] to 1.0 [4].

The vanadium distribution between crystal phases and the silicate melt is of great interest [5, 6], because the vanadium distribution during melting and crystallization in a volcanic system can be used as an oxygen barometer for natural magmas, to which the traditional methods for determining oxidation–reduction conditions cannot be applied.

According to [5], the olivine/silicate melt distribution coefficient for vanadium depends only slightly on the melt composition and, in contrast to those for the other transition elements (Cr and Ni), depends only slightly on temperature. The vanadium distribution coefficient (K) increases ten times from 0.02 to 0.2 while the oxygen fugacity decreases by five orders of magnitude below the f_{O_2} typical of the Ni–NiO buffer (ΔNNO from 0 to –5) according to the equation $K = 0.03e^{-0.547\Delta NNO}$.

Forsterite crystals doped with vanadium demonstrate luminescent properties and can be used in quantum electronics. Optical centers in forsterite with vanadium strongly emit in the near IR region and are probably related to fourfold coordinated trivalent vanadium [7, 8].

Forsterite crystals with vanadium were described in a series of publications. In particular, their mechanical properties and EPR spectra [9, 10], as well as their spectra of optical absorption and luminescence [7, 8, 11], were studied.

The results of those studies differ significantly. For example, only V^{2+} and V^{3+} were revealed by optical absorption spectra in [7]; on the other hand, only V^{4+} were found in [11]. Based on the EPR spectra, the V^{5+} was described in [10] to be predominant. These differences could be related to variations in oxidation states for various oxidation–reduction conditions. There is a disagreement between [7] and [11] in the correlation of the type of impurity center with absorption bands.

This paper is devoted to the study of vanadium distribution between the forsterite crystal and its melt, the

structural and oxidation state of vanadium in the forsterite crystals synthesized by the Czochralski technique, and their changes with variation in oxidation–reduction conditions. We studied the spectra of optical absorption and luminescence, measured the dependence of crystal density on vanadium content, and compared these parameters with a computer simulation of the crystal structure.

EXPERIMENTAL TECHNIQUE

Forsterite single crystals doped with V were grown from iridium crucibles by the Czochralski technique. Magnesium oxide and SiO_2 were taken in stoichiometric proportion. Vanadium oxides (V_2O_5 and V_2O_3) were doped. The vanadium content in the melt varied from 0.36 to 1.4 wt %. The pulling rate was 2–7 mm/h, and the rotation rate was 12 rpm. Crystals were grown in nitrogen, nitrogen with oxygen[1] (up to 2 vol %),[2] argon, and argon with hydrogen (up to 5 vol %)[3] atmospheres. The oxygen content was 0.1–0.5 vol % in pure nitrogen and 7×10^{-4} vol % in argon of special purity. Note that the addition of hydrogen increased the melt evaporation, hampered crystal growth, and could result in additional errors in *K* determination.

The vanadium content in crystals was measured with a Camebax microprobe.

The intrinsic oxygen fugacity (f_{O_2}) was determined at 800–1100°C using a high-temperature unit with two solid electrolytic cells, which are based on ZrO_2 stabilized by Y_2O_3 [12].

Absorption spectra were studied within a range of 350–1600 nm with a Perkin-Elmer Lambda 900 spectrophotometer. Luminescence was excited by an argon laser with a 514-nm wavelength and a neodymium laser with a 1064-nm wavelength and was registered by a Ge photodiode.

Relative crystal density was determined using a thermogradient flotation method. Polished samples several millimeters cubed in volume and devoid of visible defects (pores, inclusions, scratches, or cracks) were placed in a glass test-tube with flotation liquid, a mixture of methylene iodide and bromoform selected to match the forsterite density. The tube was placed in a vertical thermogradient pipe with a certain temperature difference between its ends. The thermostatic state was controlled with an accuracy of ±0.02°C using high-precision U-10 thermostats. Linear temperature (and density) distribution was maintained in the tube owing to a protective cylinder. Crystals with different densities are located at different levels in the thermogradient pipe. Using a microscope to look through a transparent slit in the protective cylinder of the thermogradient pipe, we measured the distance between the equilibrium position of the studied and reference crystals (ΔZ), which corresponds to the relative difference between their densities ($\Delta\rho/\rho$):

$$\Delta\rho/\rho = (\beta_l - \beta_c)\Delta Z dT/dZ, \quad (1)$$

where ρ is the reference sample density, β_l and β_c are the corresponding thermal expansion coefficients of the liquid and the crystal. Pure forsterite crystal was used as a reference sample. Its density was assumed to be 3.2126 g/cm^3. The sensitivity of the method depends on the temperature gradient dT/dZ and can be up to $(2–3) \times 10^{-6}$ [13], if the temperature gradient is maintained accurately enough. The measurements were performed at a temperature gradient of 0.08 K/cm. Five to ten measurements were made for each sample. The error was below $\pm 5 \times 10^{-5}$.

COMPUTER MODELING OF Mg_2SiO_4:V CRYSTAL STRUCTURE

The computer simulation of the structures of minerals and synthetic compounds is based on minimizing the structural energy of the atomic ensemble. The minimization of atomic interaction energy is successfully used to model the structures and properties of a number of crystals, for example, to compute crystal lattice defects, to localize a dopant ion in sites, to predict phase boundaries and diffusion processes, to compute crystal habits and the relaxation of crystal surfaces, and to solve other problems.

The General Utility Lattice Program (GULP) [14] was used for the theoretical simulation of a forsterite structure doped with vanadium atoms in various oxidation states. This program allows the structural parameters and optimal values of interatomic potentials to be computed by changing the site occupancy with atoms of various types; using this program it is possible to compute volumetric changes of the forsterite unit cell upon vanadium ions entering the crystal structure.

The forsterite structure was simulated using an ionic approximation. The covalence effects were partially taken into account using the potential of the O–Si–O bond angle distortion and assuming the oxygen ions to be polarized. The Madelung component of atomic interaction was computed in a reciprocal space using the Ewald method, and Buckingham potentials were used to describe short-range interactions:

$$U_{ij}(R_{ij}) = B_{ij}\exp(-R_{ij}/\lambda_{ij}) - c_{ij}/R_{ij}^6, \quad (2)$$

where R_{ij} is distance; B_{ij}, λ_{ij}, and c_{ij} are parameters of binary interaction between the *i* and *j* ions. Short-range forces were calculated for an area of radius 12 Å.

[1] The oxygen content in the ambient atmosphere is limited due to oxidation of the crucible material.

[2] The oxygen content was controlled by an OA-272 Taylor Servomech oxygen analyzer.

[3] The f_{O_2} values are approximate in this case.

Ternary interaction was considered for the directed covalent O–Si–O bond of *ijk* ions using the potential of bond angle distortion:

$$U_{ijk} = \frac{1}{2}\alpha_{ijk}(\theta_{ijk} - \theta_o)^2, \quad (3)$$

where α_{ijk} is the spring constant, θ_{ijk} is the simulated angle between bonds, and θ_o is the equilibrium tetrahedral angle (109.47°).

The polarization of an oxygen ion was considered within the shell model, where ions are described as a core concentrating the whole mass that is surrounded by a charged tightly bound shell representing the outer electron cloud. Interaction between the core with a charge of $+0.869e_0$ and a shell with a charge of $-2.869e_0$ is described using a harmonic spring constant χ_i:

$$U_i^s = (1/2)\chi_i R_i^2. \quad (4)$$

The set of potential parameters used in the calculations are listed in Table 1. The values of these parameters for pure forsterite are taken from [15]. Parameters *B* and λ were refined during structure optimization and by fitting experimental data to the atomic coordinates and unit cell dimensions for pure forsterite [16], V_2O_4 [17] and V_2O_5 [18]. The *B* and λ values for V^{2+} and V^{3+} were taken from [19].

The dissolution of vanadium with various oxidation states in a forsterite crystal can be described by the following reactions:[4]

$$Mg_{Mg}^{\times} + VO \rightleftharpoons V_{Mg}^{\times} + MgO, \quad (5)$$

$$3Mg_{Mg}^{\times} + V_2O_3 \rightleftharpoons 2V_{Mg}^{\cdot} + \nu_{Mg}'' + 3MgO, \quad (6)$$

$$2Si_{Si}^{\times} + V_2O_3 + MgO \rightleftharpoons 2V_{Si}^{\times} + Mg_i^{\cdot\cdot} + 2SiO_2, \quad (7)$$

$$Si_{Si}^{\times} + 1/2V_2O_4 \rightleftharpoons V_{Si}^{\times} + SiO_2, \quad (8)$$

$$1/2Mg_{Mg}^{\times} + Si_{Si}^{\times} + 1/2V_2O_5 \rightleftharpoons V_{Si}^{\cdot} + 1/2\nu_{Mg}'' + 1/2MgO + SiO_2. \quad (9)$$

Because the defects can form in various nonequivalent sites, we calculated the energies of defect formation (E_d) and vanadium dissolution (E_s) in different sites. In order to calculate the energy of vanadium dissolution in forsterite we also needed to know the lattice energies of pure oxides (E_{lat}). These were derived at repulsion parameters similar to those for the corresponding defects in forsterite. The use of calculated values of lattice energies allows us to expect that the errors of theoretical calculation will be compensated. The solution energies of vanadium were estimated by the following equations using Eqs. (5) and (6):

$$E_s(V^{2+}) = E(V_{Mg}^{\times}) + E_{lat}(MgO) - E_{lat}(VO), \quad (10)$$

$$E_s(V^{3+}) = E(V_{Mg}^{\cdot}) + \frac{1}{2}E(\nu_{Mg}'') + \frac{3}{2}E_{lat}(MgO) - \frac{1}{2}E_{lat}(V_2O_3). \quad (11)$$

The energy of a defect at heterovalent substitution was calculated as the sum of energies of isolated defects (dopant ion and charge compensator).

Table 1. Parameters of interatomic potentials

Bond	*B*, eV	λ, Å	*c*, eV Å^6
Si–O	1251.0218	0.3228	15.605
Mg–O	1442.84	0.2948	0
O–O	22764.3	0.149	27.88
V^{2+}–O	557.8	0.3372	
V^{3+}–O	1790.2	0.3061	
V^{4+}–O	706.88	0.384	0
V^{5+}–O	3300	0.287	0
O–Si–O	α = 2.0972 eV rad^{-2}		
O_c–O_s	χ = 74.92 eV Å^{-2}		

Note: O_c is the core and O_s is the valence shell of an oxygen ion.

RESULTS AND DISCUSSION

Vanadium ions are uniformly distributed along the crystal length (Fig. 1). The coefficient of vanadium distribution between forsterite crystal and the melt was obtained by the approximation of the data on the vanadium contents for the whole crystal to the starting crystallization point. Results of *K* determination for forster-

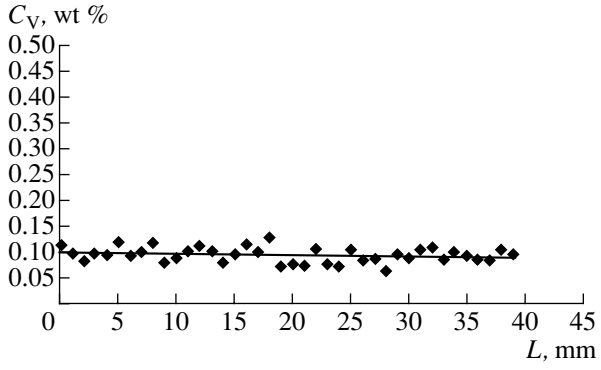

Fig. 1. Distribution of vanadium along a forsterite crystal (V content in melt is 1.45 wt %).

[4] The subscript index denotes the structural site of an atom in the crystal structure, while the superscript index denotes the excess positive (·) or negative (') charge of an atom relative to its charge in the undeformed structure (×), ν_{Mg}'' is a Mg vacancy, and $Mg_i^{\cdot\cdot}$ is a Mg interstice.

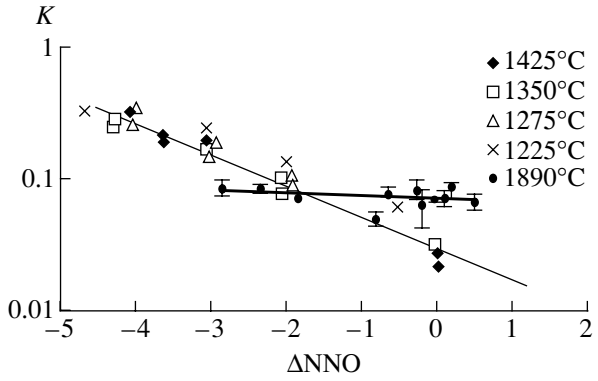

Fig. 2. Distribution coefficients of vanadium between forsterite crystal and silicate melt at various f_{O_2} (relative to the Ni–NiO buffer at different temperatures). Our data is for 1890°C, the other results are from [5].

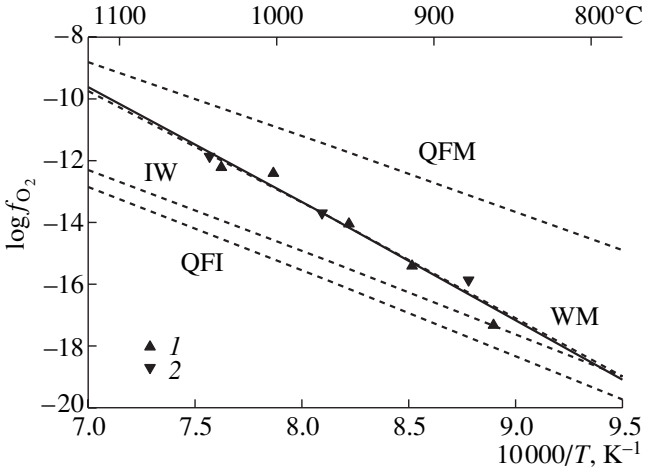

Fig. 3. Experimental dependence of $\log f_{O_2}$ on $1/T$ for pure forsterite crystal (*Fo*) grown in a nitrogen atmosphere and for a series of buffer mixtures.
(*1*) *Fo* (heating), (*2*) *Fo* (cooling), QFM is a quartz–fayalite–magnetite buffer; IW, iron–wuestite; WM, wuestite–magnetite; and QFI, quartz–fayalite–iron.

ite crystallized from the melt at 1890°C at various oxidation–reduction conditions are shown in Fig. 2. Results from [5] obtained for other temperatures and melt compositions are shown for comparison. Our data can be described by the equation $K = (0.004 \pm 0.006)$ ΔNNO + (0.070 ± 0.008). K variations within the studied range do not exceed the scatter of experimental data and, hence, it is hardly possible to distinguish any systematic enhancement in K values at low f_{O_2} values. The vanadium crystal/melt distribution coefficient for forsterite is 0.07 ± 0.01. Therefore, the assumption for vanadium K to be equal to unity made in [11] is too rough.

Data on the intrinsic oxygen fugacity of pure forsterite crystal grown in a nitrogen atmosphere are presented in Fig. 3. The linear dependence of $\log f_{O_2}$ on $1/T$ that can be described by equation $\log f_{O_2} = 14.01 - 34\,248/T$ is a good criterion to show that the sample has not suffered any alteration during measurement.

Figure 3 also shows a $\log f_{O_2}$ on $1/T$ dependence for a series of buffer systems. It is obvious that the data for forsterite are close to the parameters of a wuestite–magnetite buffer.

Figure 4 demonstrates the results of thermodynamic analysis of the vanadium oxidation state in the forsterite crystal. Stability fields for various vanadium oxides (V_2O_5, V_2O_4, V_2O_3, and VO) are drawn using data from [20]. The interval of oxygen fugacities during the growth of forsterite by the Czochralski technique, together with the melting temperature of forsterite (1890°C), are

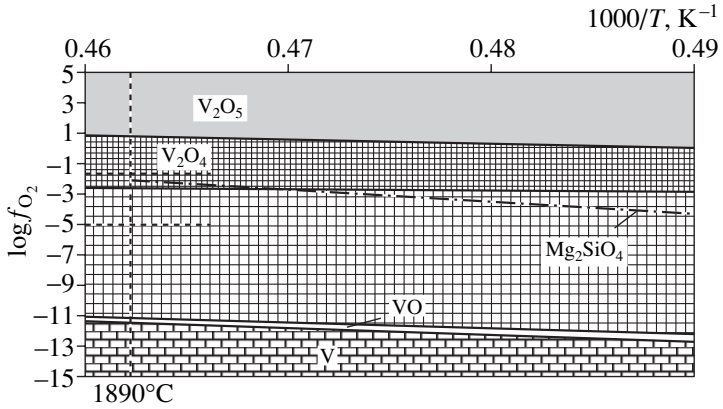

Fig. 4. Stability fields of vanadium in different oxidation states in $\log f_{O_2}$–1000/T coordinates. The dotted-dashed line denotes approximation of experimental dependence of $\log f_{O_2}$ on 1000/T for forsterite to high temperatures. Dashed lines present the interval of $\log f_{O_2}(T)$ during the forsterite synthesis by the Czochralski technique.

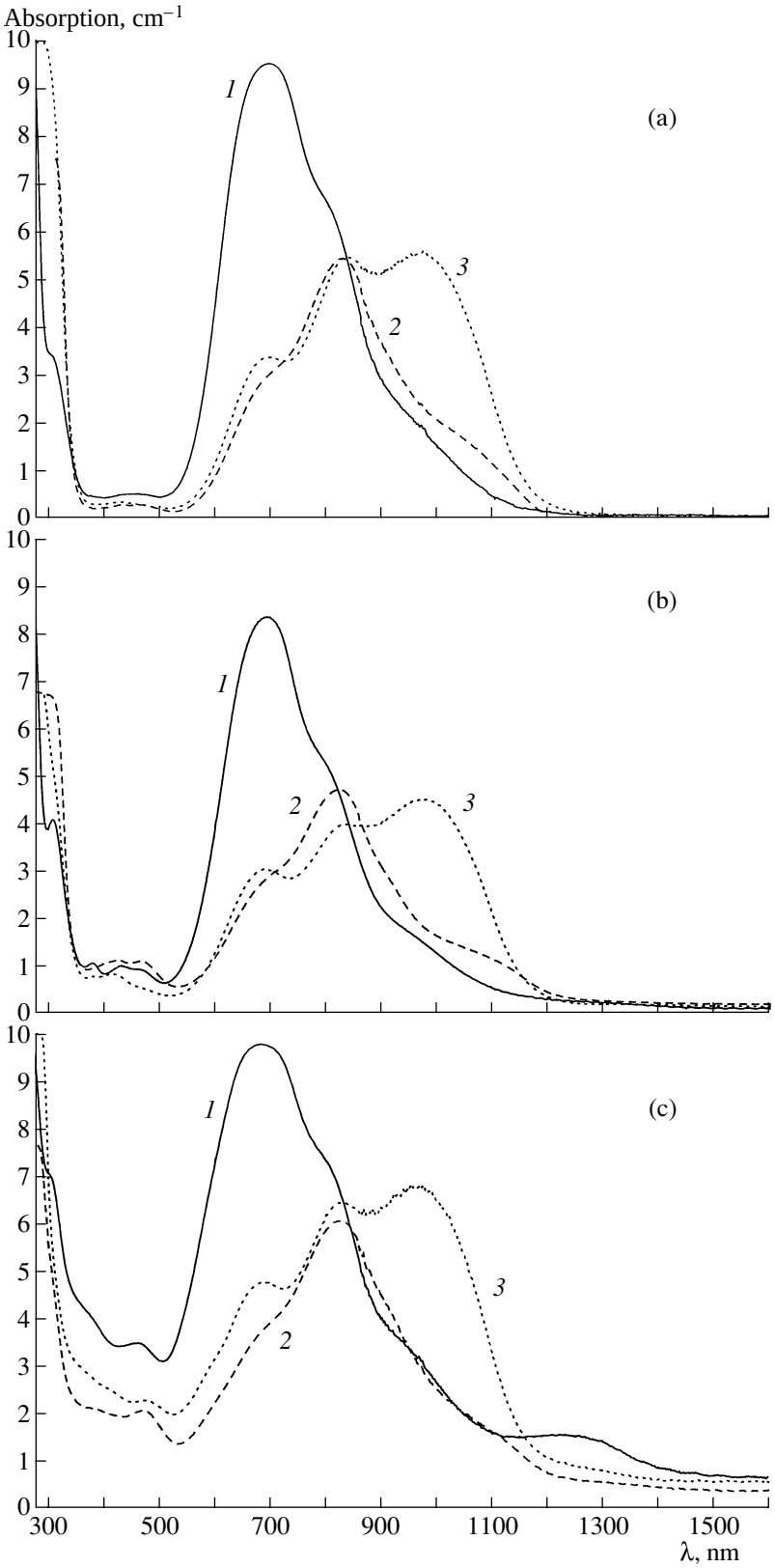

Fig. 5. Optical absorption spectra for forsterite crystals doped with V and synthesized at various oxidation–reduction conditions: (a) N_2 + 2% O_2, (b) Ar, and (c) Ar + 5% H_2. (*1*) $E \parallel a$, (*2*) $E \parallel b$, and (*3*) $E \parallel c$. Vanadium contents in crystals are 0.08 wt % for (a), 0.07 wt % for (b), and 0.12 wt % for (c).

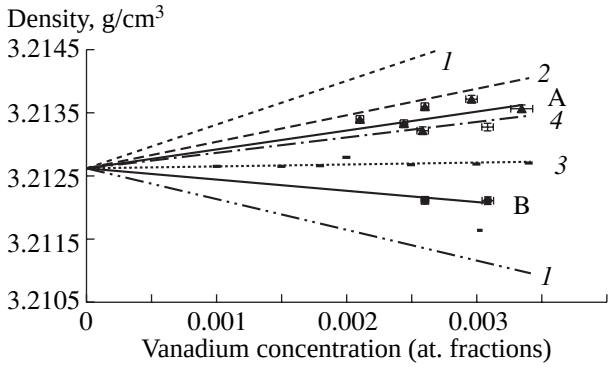

Fig. 6. Dependence of forsterite crystal densities on vanadium concentration. Simulation results are shown by dashed lines, model numbers are the same in the figure and Table 5. Experimental data for as-grown crystals (▲) and samples after oxidizing annealing (■) are approximated by solid lines A and B.

shown by dashed lines in this diagram. The oxygen intrinsic fugacities of the forsterite crystal are extrapolated to high-temperature conditions. The figure shows that V_2O_4 and V_2O_3 can be stable within the studied f_{O_2} interval at the forsterite melting temperature.

Vanadium dissolution in magnesium silicate during growth and subsequent crystal cooling can cause changes in the vanadium oxidation state. However, the occurrence of V^{2+} and V^{5+} in the forsterite crystals has a low probability. Optical absorption spectra for forsterite crystals doped with V and grown by the Czochralski technique at various oxidation–reduction conditions are shown in Fig. 5. These spectra indicate that V^{4+} replacing Si are the main absorption centers, because the continuous intensive absorption within the range of 600–1200 nm is related to the V^{4+} ion in the tetrahedral site, probably occurring as oxovanadate complex $[VO]^{2+}$ as was found in [8]. This is also consistent with data presented in [11]. The forsterite crystals synthesized in the argon atmosphere show perceptible absorption within the bands centered at 430 and 475 nm. According to [7], these absorption bands indicate the presence of V^{3+} ions in the crystals. However, luminescence typical of the V^{3+} ion in the fourfold coordination have not been registered in our samples, probably because of the low content of this ion. The annealing of forsterite crystals in equilibrium with appropriate buffers is needed for the transition of a significant amount of vanadium ions to the trivalent state. For example, annealing in a hydrogen atmosphere was used in [7] for this purpose.

Table 2. Density of forsterite crystals doped with vanadium

No.	Vanadium concentration (at. %)	Density (g/cm^3)	Growth atmosphere
1	0	3.21260	N_2
2	0.21	3.21321	N_2
3	0.24	3.21339	N_2 + 0.8% O_2
4	0.26	3.21355	N_2 + 2% O_2
5	0.26	3.21332	N_2 + 0.6% O_2
6	0.28	3.21326	Ar + 4% H_2
7	0.31	3.21359	N_2
8	0.33	3.21371	N_2 + 0.1% O_2

The results of the crystal density measurements by flotation are demonstrated in Table 2 and Fig. 6. Density variations for crystals synthesized at various f_{O_2} are insignificant and comparable with the scatter of experimental data. Thus, the dependence of crystal density on dopant concentration can be described by a common straight line.

The experimental dependence of crystal density on V concentration was compared with the computer simulation of the crystal structure to ascertain the mechanism of vanadium dissolution in forsterite. The computer simulation gave these dependences for various structural sites and oxidation states of vanadium in forsterite.

The results of the simulation of the pure forsterite structure are shown in Table 3. We calculated the atom coordinates, unit cell parameters (including volume), and crystal density. Note that the simulation and experimental data [16] are generally consistent, which justifies the model of interatomic potentials used.

When modeling the forsterite structure we also calculated the energies of defect formation and vanadium dissolution in forsterite upon the substitution of V for Mg in nonequivalent sites. This approach allowed us to choose the most probable mechanism of replacement and compensation of excess charge. The data obtained (Table 4) indicate that the replacement of Mg is energetically more favorable in the M1 site during V^{2+} dissolution and in the M2 site during V^{3+} dissolution. The formation of Mg vacancies in the M1 site is energetically most favorable for the compensation of excess positive charge during heterovalent substitution by reactions (6) and (9). For magnesium interstices $Mg_i^{\cdot\cdot}$, the sites with coordinates (0.2436; 0.25; 0.0164) are more favorable.

Simulation results of the V-doped forsterite structure are shown in Table 5. In compliance with energetically more favorable sites for defects, Mg and Si site occupancy in forsterite changes according to reactions (5)–(9). The table shows that the crystal lattice parameters varied in the fourth or even fifth decimal places. Such small variations can only be registered by high-precision experimental techniques, e.g., by the flotation method, which we used for density determinations, while the conventional X-ray technique is not appropriate for this purpose.

Table 3. Forsterite crystal structure: calculated and experimental parameters

Parameter	Calculated			Experimental [16]		
a, Å	10.2573			10.18		
b, Å	5.9969			5.976		
c, Å	4.7296			4.746		
V, Å^3	290.9256			288.6		
ρ, g/cm^3	3.2126			3.2391		
Space group *Pnma*						
Atom coordinates (Z = 4)	*x*	*y*	*z*	*x*	*y*	*z*
Mg(M1)	0.0000	0.0000	0.0000	0.0000	0.0000	0.0000
Mg(M2)	0.2844	0.2500	0.9998	0.2772	0.2500	0.9914
Si	0.0986	0.2500	0.4432	0.0939	0.2500	0.4261
O(1)	0.0929	0.2500	0.7781	0.0919	0.2500	0.7661
O(2)	0.4550	0.2500	0.2104	0.4469	0.2500	0.2202
O(3)	0.1648	0.0390	0.2962	0.1628	0.0333	0.2777

Table 4. Energies of formation of intrinsic and extrinsic defects and solution energy of vanadium in forsterite in different sites

Site	M1	M2	(0.5; 0; 0)	(0.2436; 0.25; 0.0164)
Defect	Energy of defect formation (E_d), eV			
v''_{Mg}	25.50	28.05		
$Mg_i^{\bullet\bullet}$			–8.75	–17.10
	E_d, eV		E_s, eV	
	M1	M2	M1	M2
$V^{\times}_{Mg}$	0.06	0.16	0.51	0.61
$V^{\bullet}_{Mg}$	–22.23	–22.70	3.84	3.37

The calculated variations of forsterite crystal densities with different vanadium concentrations are shown in Fig. 6 for all the substitution mechanisms discussed. The experimental data are most consistent with data calculated for Si by V^{4+} replacement. Results of spectroscopic investigations also indicate that vanadium occurs in forsterite crystals generally in a tetravalent form.

After comparing the experimental and calculated data with the crystal densities, we suggest that the crystals do not have a significant content of V^{5+} ions.

In order to prove this hypothesis we performed oxidizing annealing of the crystals at 1200°C and $\log f_{O_2}$ = –0.01 in sealed quartz ampules filled with oxygen. Annealing lasted 800 h.

The annealing of crystals in an oxygen atmosphere led to significant changes in their densities. The experimental dependence of crystal density on V concentration approached that calculated for crystals with V^{5+} ions. Thus, V^{5+} did not exist in a notable amount after the crystal synthesis and vanadium atoms were significantly oxidized during annealing.

Thus, forsterite crystals synthesized by the Czochralski technique contain mostly V^{4+}. The crystals formed at lower f_{O_2} also include V^{3+}. However, the concentrations of these ions are small and do not cause significant changes in the crystal densities and distrubution coefficients of vanadium between crystal and melt. Their existence is also not seen in the luminescence spectra. The reduction of a sufficient vanadium amount to the trivalent state (so that it becomes pronounced in the luminescence spectra) or the oxidation of initial vanadium to a pentavalent state can be

Table 5. Simulation of forsterite crystal doped with vanadium

No.	Admixture dope	Defects	Vanadium concentration (at. fractions)	*a*, Å	*b*, Å	*c*, Å	*V*, Å^3	ρ, g/cm^3
1	V^{2+}	$V^{\times}_{Mg}$(M1)	0.001	10.25732	5.99682	4.72951	290.91797	3.21331
			0.002	10.25734	5.99672	4.72945	290.91049	3.21400
			0.0034	10.25738	5.99659	4.72936	290.90002	3.21497
2	V^{3+}	$V^{\bullet}_{Mg(M2)}$, $1/2\nu''_{Mg(M1)}$	0.001	10.25741	5.99664	4.72960	290.91763	3.21304
			0.002	10.25753	5.99636	4.72964	290.90983	3.21345
			0.0034	10.25769	5.99597	4.72969	290.89890	3.21404
3	V^{3+}	V'_{Si}, $1/2Mg^{\bullet\bullet}_i$	0.001	10.25819	5.99677	4.73041	290.99597	3.21264
		(0.2436; –0.25; 0.0164)	0.002	10.26192	5.99571	4.73050	291.05565	3.21278
			0.0034	10.26086	5.99619	4.73239	291.16493	3.21269
4	V^{4+}	$V^{\times}_{Si}$	0.001	10.25745	5.99701	4.72983	290.95059	3.21286
			0.002	10.25762	5.99710	4.73008	290.97572	3.21311
			0.0034	10.25785	5.99724	4.73044	291.01091	3.21345
5	V^{5+}	$V^{\bullet}_{Si}$	0.001	10.25769	5.99689	4.73049	290.99234	3.21212
			0.002	10.25809	5.99686	4.73141	291.05905	3.21163
			0.0034	10.25864	5.99682	4.73269	291.15138	3.21095

achieved by annealing as-grown crystals under reducing or oxidizing conditions, respectively.

CONCLUSION

Our study revealed that vanadium segregation between a forsterite crystal and the melt is characterized by a distribution coefficient of 0.07, which does not change significantly with variations in oxidation–reduction conditions. Based on spectra of optical absorption and the luminescence of V-doped forsterite crystals, measurements of crystal density by the high-precision flotation method, computer simulation of the crystal structure, and thermodynamic analysis, we concluded that vanadium is incorporated in the forsterite crystals mostly as V^{4+} replacing Si.

Crystals with optical centers emitting in the near IR region and being ascribed to fourfold coordinated trivalent vanadium did not form in our experiments. The oxidation state of vanadium can be changed to V^{3+} or V^{5+} by annealing the crystals under reducing or oxidizing conditions, respectively.

ACKNOWLEDGMENTS

The authors thank B.N. Ryzhenko for his help in the thermodynamic analysis of vanadium oxidation state, and I.Ch. Avetisov, A.V. Gaister, and S.V. Lavrishchev for their help in the experimental work and the discussion of results.

The study was supported by the Russian Foundation for Basic Research (projects 99-05-65139 and 99-02-18456), by the Federal Program "State Support of Integration of Higher Education and Fundamental Science" (projects 683 and A0080), and by the Federal Program for the Support of Leading Scientific Schools (project 00-15-98582).

REFERENCES

1. Shannon, R.D., Revised Effective Ionic Radii and Systematic Studies of Interatomic Distances in Halides and Chalcogenides, *Acta Crystallogr., Ser. A*, 1976, vol. 32, pp. 751–767.
2. Glazunov, O.M., Mekhonoshin, A.S., and Zakharov, M.N., *Geokhimiya elementov gruppy zheleza v endogennom protsesse* (Geochemistry of Iron-Group Elements in the Endogenous Process), Novosibirsk: Nauka, 1985.
3. Irving, A.J., A Review of Experimental Studies of Crystal/Liquid Trace Element Partitioning, *Geochim. Cosmochim. Acta*, 1978, vol. 42, pp. 743–770.
4. Jones, J.H., Experimental Trace Element Partitioning, *Rock Physics and Phase Relations: A Handbook of Physical Constants*, Ahrens, T.J., Ed., 1995, pp. 73–104.
5. Canil, D., Vanadium Partitioning and the Oxidation State of Archean Komatiite Magmas, *Nature* (London), 1997, vol. 389, pp. 842–845.
6. Canil, D., Vanadium Partitioning between Orthopyroxene, Spinel, and Silicate Melt and the Redox States of Mantle Source Regions for Primary Magmas, *Geochim. Cosmochim. Acta*, 1999, vol. 63, no. 3/4, pp. 557–572.

7. Avanesov, A.G., Dvornikova, V.G., Zhorin, V.V., *et al.*, Spectroscopy of Forsterite Single Crystals Doped with Nickel and Vanadium Ions, *Zh. Prikl. Spektrosk.*, 1993, vol. 59, nos. 1–2, pp. 152–154.
8. Veremeichik, T.F., Gaister, A.V., Konarev, P.V., *et al.*, Valences and Structural Sites of Minor Vanadium Ions in Forsterite Crystals, *Tezisy dokladov Vtoroi natsional'noi konferentsii po primeneniyu rentgenovskogo, sinkhrotronnogo izluchenii, neitronov i elektronov dlya issledovaniya materialov* (Abstr. Second National Conf. Applied X-ray and Synchrotron Radiation, Neutrons, and Electrons for Studying Materials), Moscow: Inst. Crystallogr., Russ. Acad. Sci., 1999, p. 352.
9. Ricoult, D.L. and Kohlstedt, D.L., Creep Behavior of Single Crystals of Vanadium-Doped Forsterite, *J. Am. Ceram. Soc.*, 1986, vol. 69, pp. 770–774.
10. Mackwell, S.J. and Kohlstedt, D.L., High-Temperature Deformation of Forsterite Single Crystals Doped with Vanadium, *Phys. Chem. Miner.*, 1986, vol. 13, pp. 351–356.
11. Brunold, T.S., Gudel, H.U., and Kaminski, A.A., Optical Spectroscopy of V^{4+} Doped Crystals of Mg_2SiO_4 and Ca_2GeO_4, *Chem. Phys. Lett.*, 1997, vol. 271, pp. 327–334.
12. Kadik, A.A., Zharkova, E.V., Kovalenko, V.I., and Ionov, D.A., The Redox Conditions of the Upper Mantle: Experimental Studies of Oxygen Fugacity of Peridotite Xenoliths from Shavaryn-Tsaram Volcano, Mongolia, *Geokhimiya*, 1988, no. 6, pp. 783–793.
13. Andreev, G.A., The Floatation Method for Measuring Density of Solids and Its Application, *Monokrist. Tech.*, 1973, issue 2, pp. 1–10.
14. Gale, J.D., GULP: A Computer Program for the Symmetry-Adapted Simulation of Solids, *J. Chem. Soc., Faraday Trans.*, 1997, vol. 93, pp. 629–637.
15. Sanders, M.J., Leslie, M.J., and Catlow, C.R.A., Interatomic Potentials for SiO_2, *J. Chem. Soc. Chem. Commun.*, 1984, vol. 18, pp. 1271–1273.
16. Hazen, R.M., Effects of Temperature and Pressure on the Crystal Structure of Forsterite, *Am. Mineral.*, 1976, vol. 61, pp. 1280–1293.
17. Rogers, K.D., An X-ray Diffraction Study of Semiconductor and Metallic Vanadium Dioxide, *Powder Diffr.*, 1993, vol. 8, no. 4, pp. 240–244.
18. Engalbert, R. and Galy, J., A Refinement of the Structure of V_2O_5, *ACSCE*, 1986, vol. 42, pp. 1467–1469.
19. Lewis, G.V. and Catlow, C.R.A., Potential Models for Ionic Oxides, *J. Phys. C: Solid State Phys.*, 1985, vol. 18, pp. 1149–1161.
20. Kulikov, I.S., *Termodinamika oksidov* (The Thermodynamics of Oxides), Moscow: Metallurgiya, 1986.